



Wire Electric Discharge Machining at Different Slant Angles during Slant Type Taper Profiling of Microfer 4722 Superalloy

I.V. Manoj and S. Narendranath

Submitted: 29 May 2021 / Revised: 26 July 2021 / Accepted: 13 August 2021 / Published online: 31 August 2021

Wire electric discharge machining (WEDM) is nonconventional machining that provides machining solutions irrespective of the material hardness. In the present study, a simple profile was machined on Microfer 4722 at different slant angles using to know the effect of machining parameters. A unique method of obtaining taper components was employed by slant type taper fixture to avoid the disadvantages of the conventional method. The profiling speed, profile roughness, profiling error (Corner error), recast layer thickness, micro-hardness, microstructural and metallurgical changes of the machined component were investigated. As the taper of the component increases the profile roughness, corner error increases although profiling speed decreases. It is observed that recast layer thickness decreases as the taper of the component increases. A contrasting phenomenon is observed in the case of hardness at the WEDM surface. The metallurgical changes like the addition of Cu, Zn and O in the nickel-based alloy after machining from WEDM at different slant angles are highlighted. It is observed that residual stress decreased as the slant angles increased from 0° to 30° during slant type profiling.

Keywords microfer 4722, micro-hardness, profiling error (corner error), recast layer thickness, residual stress, slant type tapering

1. Introduction

Nickel-based alloys are hard to machine, high-temperature alloys having various applications. They exhibit superior properties at elevated temperature, high melting point, excellent resistance to corrosion, high toughness and ductility, thermal shocks, thermal fatigue and erosion. Conventional machining is not always the excellent solution for machining such alloys due to high surface roughness, surface defects, residual stress, and tool damage (Ref 1-3). Wire electric discharge machining is a process that removes the material by the erosion of debris and melting of the workpiece by electric sparks between the wire and the workpiece. This material removal mechanism enables the machining of materials of variable hardness. So many hard to machine materials like nickel-based alloys, shape memory alloys, titanium and cobalt-based alloys can be machined (Ref 4-6). Microfer 4722 is a unique group of nickel-based alloys that can be precisely machined by WEDM which is used in many applications in aerospace, marine, chemical, tool and die industries, etc. These applications in industries demand intricateness and dimensional accuracies in components having taper complex shapes where WEDM gains more significance (Ref 7, 8). Many changes occur in workpiece, and many researchers have highlighted by different researchers as fol-

lows. Sharma et al. have highlighted the metallurgical and microstructural changes due to the variations in cutting parameters. The WEDMed surface was degraded by the presence of Cu, Zn and O which was transferred from the wire (Ref 9). Bisaria & Shandilya have investigated metallographic changes of Ni55.95Ti44.05 shape memory alloy. It was found that Ti, Ni, Zn, and Cu were deposited in the parent material during machining of shape memory alloy using brass wire as an electrode (Ref 10). Soni et al. have identified the formation of different layers after machining in the wire EDMed surface of TiNiCo shape memory alloys which causes variation in micro-hardness (Ref 11). Muralova et al. have evaluated the influence of cutting direction on semi-finished products in terms of defects of the sub-surface area. Effect of machining parameters on defects like cracks with burned cavities with residual stress have been reported as this may lead to poor machined surface (Ref 12). Sun et al. reported low-speed WEDT is a superior machining process in the fabrication of microelectrodes due to its non-contact removal mechanism. Finally, by the microstructure analysis, it was concluded that the surface quality machined by LS-WEDT after finishing trim cut is better than LS-WEDM (Ref 13). Hatami et al. observed the diffusion of Cu and Zn into the WEDMed surface of powder metallurgical tool steels although the other parameters like surface roughness and residual stress exhibited an insignificant change even after four passes of WEDM (Ref 14). Ahmad and Fitzpatrick have investigated the WEDM cutting parameters to identify the optimum conditions for the contour method residual stress measurements. This contour method improved the residual stress magnitude up to 150 MPa which was also validated by x-ray diffraction, incremental center hole drilling, and neutron diffraction (Ref 15). Bhattacharya et al. have investigated the cutting process, microstructure on or under the surface, and the surface finish with the nature and the morphology of the phases. Based on different microstructural features, thermal model was formulated which was also used

I.V. Manoj and S. Narendranath, Department of Mechanical Engineering, National Institute of Technology Karnataka, Surathkal 575025, India. Contact e-mail: vishalmanojvs@gmail.com.

for the prediction of surface finish (Ref 16). Bisaria and Shandilya have reported surface morphology, three-dimensional surface topography, recast layer, phase analysis, and micro-hardness for WEDMed Ni55.95Ti44.05 shape memory alloy. The metallurgical changes of the WEDMed surface were highlighted by x-ray diffraction. This resulted in decreased micro-hardness at the machined region and increased 1.98 times as moved toward the bulk material from the machined region (Ref 17). Huang et al. have explored the behavior of quenched and tempered martensitic stainless steel of rough-cut WEDMed surface. It was concluded that heat-treatment conditions influenced surface intergranular cracks, recast layer and heat-affected zone of the WEDMed surface (Ref 18).

The research goal of the study was to perform a taper profiling operation using Microfer 4722 super alloy and to quantify the effects of performance parameters used of machining on different tapered components. Many response parameters like profiling speed, profile roughness, profiling error (Corner error), recast layer thickness, micro-hardness, and residual stress with metallurgical changes were investigated. A unique way of machining a taper profile surface was attempted using slant type taper fixture to avoid conventional demerits of tapering in WEDM. The effect of slant angles with input parameters like wire guide distance (WGD), corner dwell time (CDT), wire offset (WO) and cutting speed override (CSO) on output responses was explored. One factor at a time (OFAT) experimental method was followed, and this shows specific variation in response for different input parameters. It is observed that as the slant angles increase the profile roughness increases and corner error increases although profiling speed decreased. The micro-hardness at the machined surface increased as the slant angles increased, but the recast layer thickness and residual stress decreased. X-ray diffraction (XRD) and energy-dispersive x-ray analysis (EDS) analysis were performed at each slant angled component for the highest profiling speed to explore the effects of machining.

2. Experimental Particulars

2.1 Material

Microfer 4722 is a nickel-chromium-iron-molybdenum superalloy having high mechanical properties, oxidation resistance, fabricability and high-temperature strength. Its density at 72 °F (23 °C) is 8.22 g/cm³, tensile strength is 755 Mpa and elastic modulus is 205Gpa. It possesses exceptional strength and oxidation resistance up to 1200 °C. It is extremely resistant to stress-corrosion cracking which has much application in chemical and petrochemical applications (Ref 19). It is used extensively in high-temperature gas turbine engines so it is also known as turbine alloy. The composition of the as-received alloy was tested from optical emission spectrometry (SpectraMax 130779) at Quality Test Laboratory, Mumbai, India, is

Table 1 Chemical composition of Microfer 4722 superalloy

%	C%	Si%	Mn%	P%	S%	Cr%	Mo%	Fe%	Co%	W%	Ni%
C	0.06	0.21	0.65	0.027	0.01	20.65	8.24	18.05	0.69	0.29	50.88

*C-Composition.

shown as in Table 1. The as-received plate is cut to 260 mm × 22 mm × 10 mm for machining the slot which was programmed. As established from the literature, the superalloy was solution heat-treated at 2150 °F (1177 °C) and rapid cooled. The holding time of 1hr per inch of the section was followed (Ref 20).

2.2 Machining Details

Figure 1 shows the machining method followed in the square profiling of sides 1 mm, 3 mm and 5 mm which were programmed as shown in for machining. The ELCAM was used for modelled and simulation in CNC software. The software generates NC codes in the form of .WC files for the required machining conditions. This .WC file is loaded in Electronica 'ELPLUS 15 CNCWEDM' where the wire machines the programmed path. The zinc-coated copper wire of diameter 0.25 mm was used as an electrode for machining the profile on Microfer 4722. The deionized water was used as dielectric fluid throughout the investigation. A fixture made of aluminum H9 series was used to tilt the workpiece to different slant angles as shown in Fig. 1(a). The programmed profile was machined at different slant angles namely 0°, 15° and 30° on a workpiece placed on an angular plate of fixture. Figure 1(b) shows the different positions of the workpiece during profiling. The angular plate is anchored at a specific angle with the help of the slots provided in the side plate. The whole setup with the workpiece was mounted on the WEDM table for profiling during the study. It can also be observed that as the slant angles increase the thickness (*t*) of the metal to be machined also increases.

2.3 Characterization Technique

For the present investigation, the profiling speed was calculated as the average of all the instantaneous profiling speeds which is recorded from the WEDM setup during profiling. The average of 5 profile roughness values was measured using the 'Mitutoyo SJ-301' profile roughness tester. For profiling error (Corner error), surface morphology and recast layer thickness images were obtained from 'JEO JSM-6368OLA' and 'Hitachi SU 3500' scanning electron microscope (SEM) at 100X, 1000X and 500X magnification, respectively. Image J software is used to calculate the profiling error (Corner error) in terms of area for the second corner of the profile and recast layer thickness. This Image J software can measure the areas and thickness from the SEM images recorded (Ref 10). The micro-hardness is measured using 'OMNI TECH MVHS-AUTO' Vicker's micro-hardness tester and the micro-hardness of the base metal is 212Hv. The x-ray diffraction of 'Empyrean III' was performed on the machined samples and analyzed using X'PERT High Score Plus software. The residual stress measurement was done using the XRD technique in IIT Bombay.

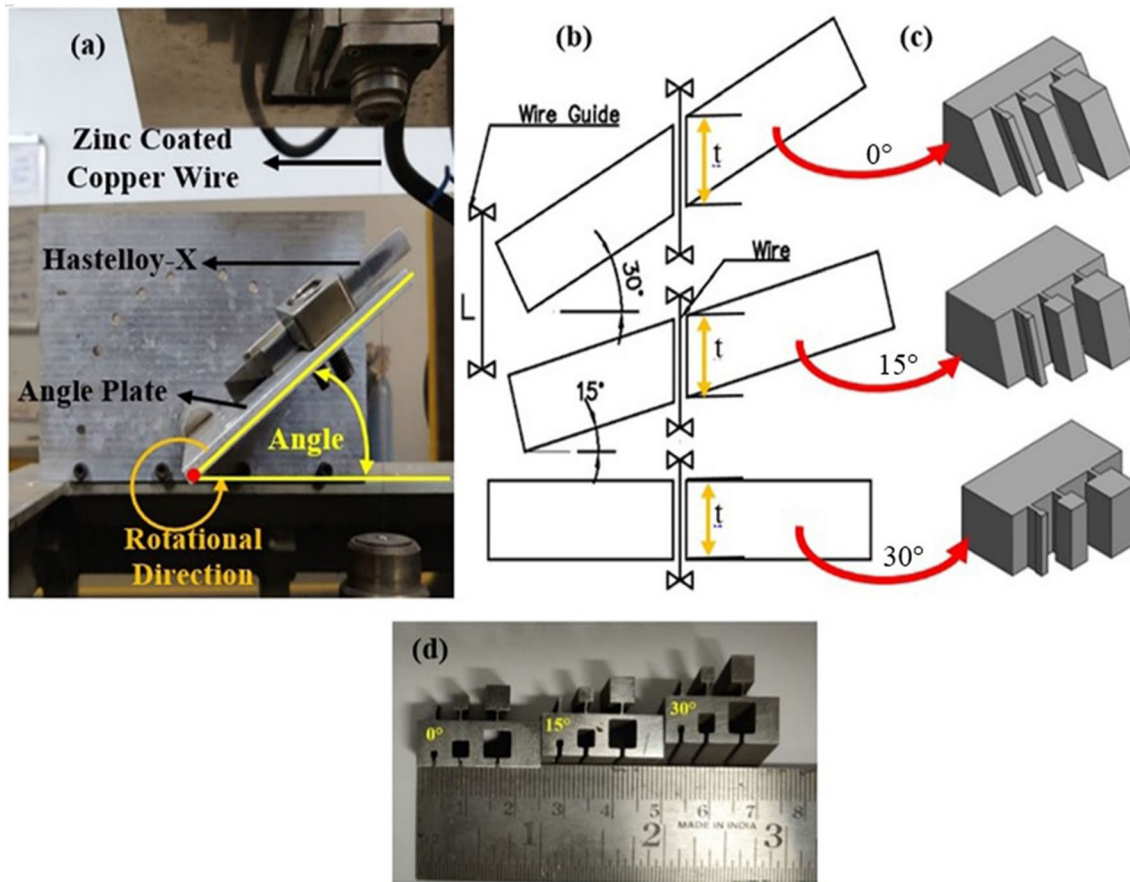


Fig. 1 (a) Fixture on WEDM table (b) Workpiece position at different slant angles (c) Machined component at the isometric view (d) WEDM tapered components

Table 2 WEDM constant and profiling parameters

Constant parameters				
WEDM parameters	Settings			
Pulse off time, μs	44			
Servo feed, mm/min	20			
Wire feed, m/min	6			
Pulse on time, μs	115			
Servo voltage, V	40			
Profiling parameters				
Wire guide distance, mm	90	100	110	120
Cutting speed override, %	31	54	77	100
Wire offset, μm	0	40	80	120
Corner dwell time, s	0	33	66	99

2.4 Machining Parameters

Based on the initial experiments on the workpiece and tool combinations that were performed, the machining parameters were selected. The basic constant parameters were maintained throughout the experimentation as shown in Table 1. Table 2 shows the profiling parameters like WGD, CDT, WO and CSO that were employed during profiling. These parameters were chosen based on the machining capability and initial experi-

ments. The WGD was chosen as such that the profiling could be easily performed with minimal vibration for all three slant angles as shown in Table 2. OFAT was followed in the experimental approach. In this approach, apart from one parameter others were maintained to minimal (level 1) to know the individual effects on response parameters. Figure 1(d) shows the different taper square profiles of 10mm thickness obtained after profiling.

3. Results and Discussion

3.1 Analysis of Profiling Speed

The behavior of profiling speed for the different input parameters like WGD, CDT, WO and CSO was as shown in Fig. 2(a)-(d). The WGD is the distance between the upper guide and the lower guide. As the WGD parameter increases, the tension in the wire tends to lower and the tendency of wire vibration also increases (Ref 21). This wire vibration decreases the profiling speed due to its chaotic nature. So there is a decrease in profiling speed as shown in Fig. 2(a). Figure 2(b) shows the profiling speed variations with the CDT parameter. The CDT parameter mainly affects the corners during complex shape profiling (Ref 22). It is seen a very low variation of profiling speed as the CDT parameter increases. This effect is due to machining errors. The CDT parameter was found to not affect profiling speed. The WO parameter is the fixed perpendicular distance from the programmed profile. According to the observations by Habib and Okada, as the WO parameter increases the wire vibration decreases because the wire has to cover the larger part of profile circumference (Ref 23). This increases the profiling speed as wire vibration decreases as shown in Fig. 2(c). The CSO is an online parameter that varies the profiling speed without altering the machining parameter (Ref 24). Figure 2(d) shows the variation of the CSO parameter on profiling speed. The CSO parameter controls the discharge during machining which in turn controls the profiling speed. So as the CSO parameter was increased the profiling speed also increased due to the increase in discharge energy (Ref 22,24). It can be observed from all the plots the 0° slant angles produced the highest profiling speed followed by 15° and 30°. This effect of the decrease in profiling speed with an increase in slant angles was observed because of the increase in cutting thickness. As the slant angles increase, the cutting thickness also increases. As the cutting thickness increases, the discharge energy during machining gets distributed (Ref 25). This decreases the profiling speed as the discharge energy

remains fixed for a parameter. So the 30° slant angle has the least profiling speed as it has the highest thickness, whereas the 0° slant angles have the highest profiling speed due to the lowest cutting thickness.

3.2 Analysis of profile roughness

The variation of profile roughness with different input parameters was highlighted as shown in fig. The profile roughness increases as the WGD parameter increases as shown in Fig. 3(a). As the WGD parameter increases, the wire tension decreases (Ref 26,27). Chaudhary et al. have noticed in their investigation that as the wire tension decreases the impact force on the wire due to the frequency by spark is very high (Ref 21). So the wire vibration increases which gives multiple irregulars sparking on the same machining surface. Therefore, the profile roughness increases with the WGD parameter as wire vibration due to the multiple irregular sparking effect (Ref 23). Figure 3(b) shows the variation of CDT parameters on profile roughness. It can be observed that as the CDT parameter affects the corner of the complex profiles, but it does not affect profile roughness (Ref 22). It can be observed from Fig. 3(c) that as the WO parameter increases the profile roughness also increases. As observed from Fig. 2(c) the profiling speed increases with an increase in the WO parameter. As profiling speed increases, the sparking also increases yielding higher profile roughness (Ref 21, 26). This is due to the formation of higher craters, bigger micro-globules, modules, holes, etc., clearly shown in Sect. 3.4. So the profile roughness also increases as the WO parameter increases as shown in Fig. 3(c). The WO parameter controls the perpendicular distance from the programmed profile. As the perpendicular distance increases, the wire vibration decreases which gives higher profiling speed, in turn, increasing profile roughness (Ref 24). The CSO parameter controls the discharge energy during machining (Ref 22, 25). As the discharge energy increases, the profiling speed increases giving a rough surface. So the profile roughness increases as the CSO parameter increases which are observed in Fig. 3(d). It can be observed that the profile roughness of 30° slant angles was recorded highest followed by 15° than 0°

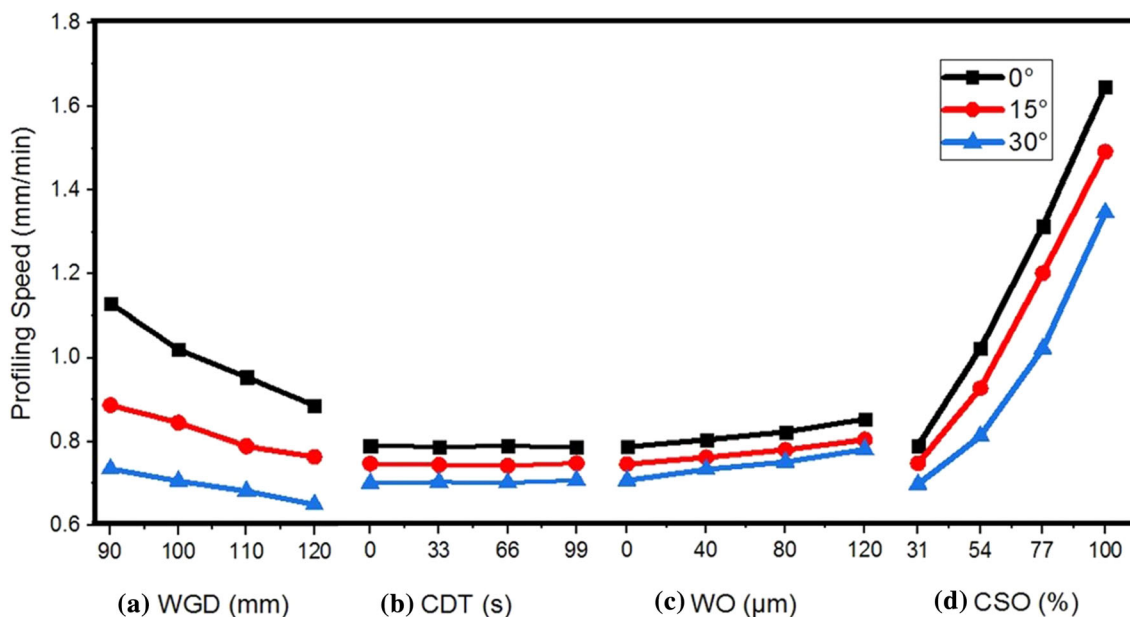


Fig. 2 Effect of (a) WGD, (b) CDT, (c) WO and (d) CSO on profiling speed

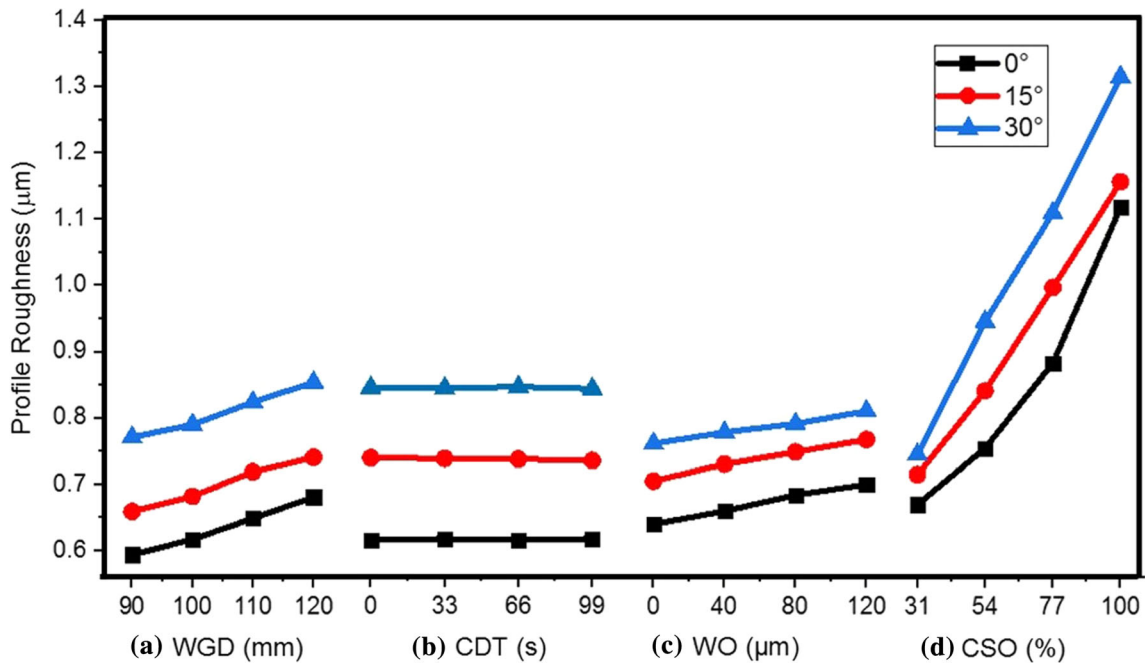


Fig. 3 Effect of (a) WGD, (b) CDT, (c) WO and (d) CSO on profile roughness

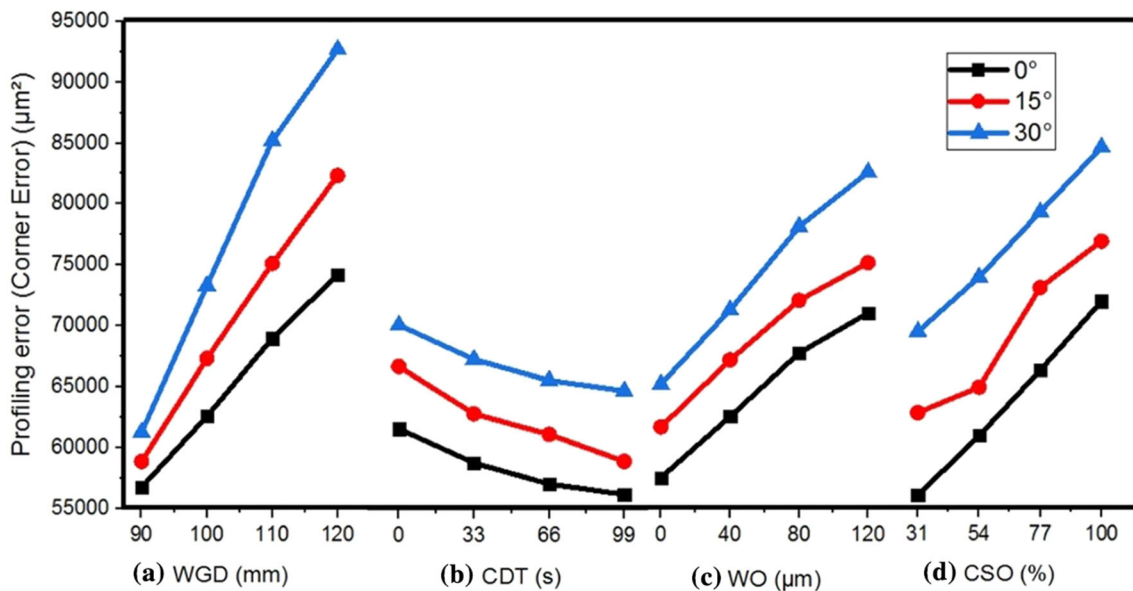


Fig. 4 Effect of (a) WGD, (b) CDT, (c) WO and (d) CSO on profiling error

slant angles. As the cutting thickness increases, the profile roughness also increased although the profiling speed decreased. This behavior was observed due to the increased discharge energy and the variation in gap voltage. This increase in profile roughness at lower profiling speed was due to the high cutting thickness as reported by Manoj et al. (Ref 26).

3.3 Analysis of Profiling Error (Corner Error)

The profiling error is measured by Image J software from the SEM images at various parameters of profiling. Figure 4(a)-(d) shows the variation of profiling error for different input parameters during machining of a tapered profile. The WGD parameter is the wire distance that was used for machining. As

WGD increases, the tendency of the wire to deflect also increases due to the lower tension (Ref 26, 27). With an increase in wire deflection, the profiling error also increases (Ref 28). So as WGD increases, the profiling error also increases as highlighted in Fig. 4(a). The CDT parameter is specifically for the machining of complex corners (Ref 22). As the CDT increases, the profiling error decreased as shown in Fig. 4(b). The CDT parameter makes the wire dwell at a specific coordinate to decrease the wire lag. The wire deflection is the main reason for wire lag where the wire remains behind the actual coordinates (Ref 22). As the wire lag decreases, the profiling error also decreases (Ref 28, 29). Figure 4(c) explains the behavior of profiling error with the increase in the WO

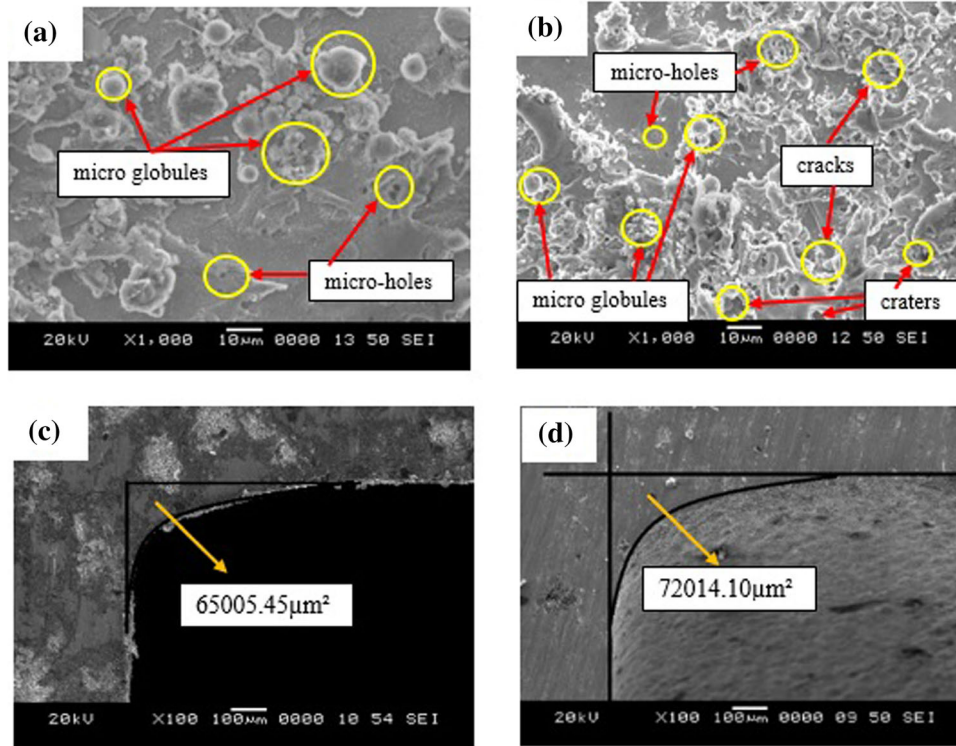
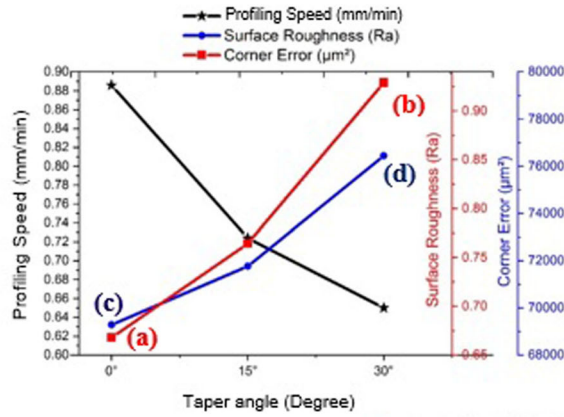


Fig. 5 Variation of profiling speed, profiling error, profile roughness and SEM images of profiling error at (a) 0°, (b) 30° slant angles and machined surface at (c) 0°, (d) 30° slant angles for lowest profiling speed parameters (WGD = 120 mm, CDT = 0 s, WO = 0 µm, CSO = 31%)

parameter. Saheb and Okada have observed that as the WO parameter increases the wire deflection also increases (Ref 24). This wire deflection increases with the WO parameter as the wire has to machine a higher circumference than the programmed profile. This increases the profiling error due to the increase in wire deflection. The CSO parameter controls the discharge energy which in turn governs the profiling speed. It was observed that as the CSO parameter increase the profiling error also increased. This phenomenon was noticed due to the increase in wire lag. As the CSO increases, the wire has to machine faster due to the increase in discharge energy (Ref 22, 25). But it is observed that the wire deflected causing wire lag as it could not travel as fast as the wire guide. This increased the profiling error as the CSO parameter increased as shown in Fig. 4(d). It can be observed the 30° slant angles yielded a higher profiling error than the 0° slant angles. This effect was observed due to her cutting thickness as the workpiece is tilted

in Fig. 1(b). As workpiece/cutting thickness increases, the wire tend to deflect more which caused wire deflection (Ref 27). So as the wire deflection was highest at 30° giving the highest profiling errors followed by 15° and 0° slant angles as shown in Fig. 4.

3.4 Variation of Profiling Speed, Profile Roughness and Profiling Error at Different Slant Angles

Figure 5 and 6 shows the variation of profiling speed, profiling error and profile roughness at different slant angles for the lowest and highest profiling speed parameters. It can be seen that both parameters have similar effects on the response parameter. As the slant angle increases, the cutting/workpiece thickness also increases. With an increase in cutting thickness, the profiling speed decreases as the discharge energy gets distributed. This increase in cutting thickness in turn affecting the profiling speed due to a decrease in the rate of length of cut

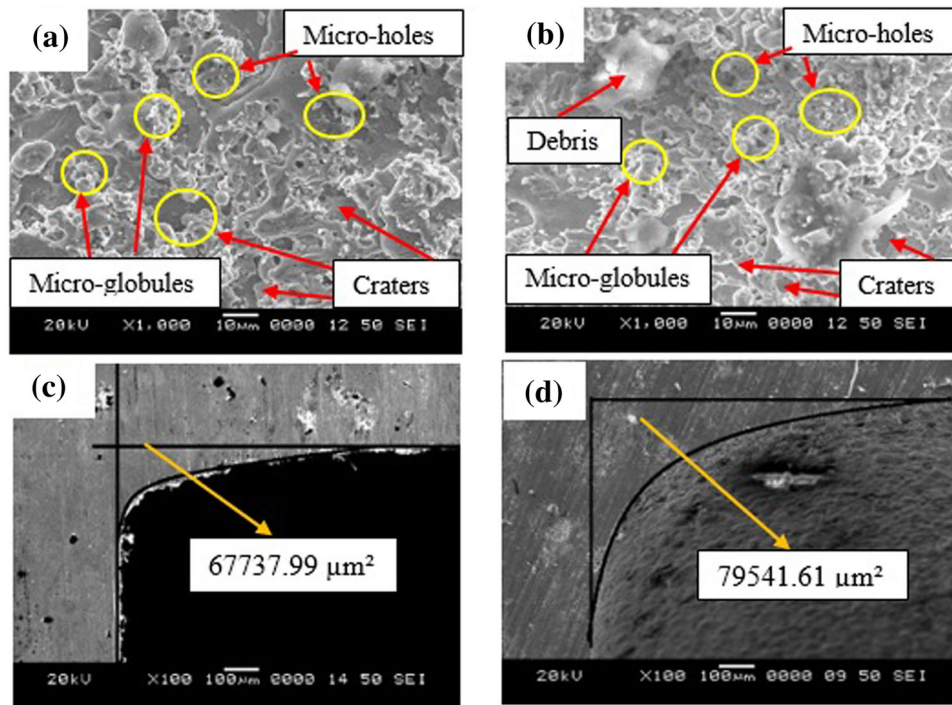
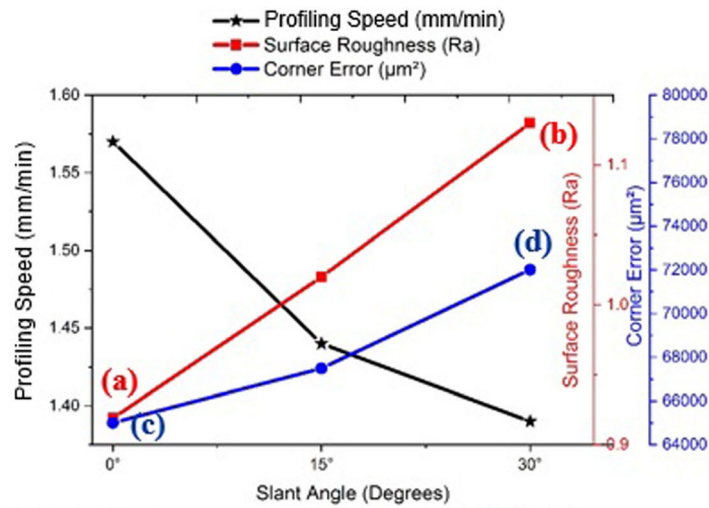


Fig. 6 Variation of profiling speed, profiling error, profile roughness and SEM images of profiling error at (a) 0°, (b) 30° slant angles and machined surface at (c) 0°, (d) 30° slant angles for highest profiling speed parameters (WGD = 90 mm, CDT = 99 s, WO = 120 µm, CSO = 100%)

(Ref 25, 26). The profiling speed was found to be 1.57 mm/min, 1.44 mm/min and 1.39 mm/min for 0°, 15° and 30° slant angles, respectively, for the highest cutting parameters. For lowest cutting parameters, it was 0.886 mm/min, 0.764 mm/min and 0.65 mm/min at respective slant angles.

In case of profiling error, due to the increase in thickness, the wire deflection also increased. This increased the wire lag leading to higher profiling error. It can be seen in both Fig. 5 and 6 at the highest and lowest parameters the profiling speed decreased and the profiling error increases as the slant angles increased which contrasting with behavior reported by Selvakumar et al. (Ref 30). The SEM images in Fig. 5 and 6 show the profiling error at the lowest and highest profiling speed parameters. At the lowest cutting parameters, it was found to be

65005.45 µm², 67487.25 µm² and 72014.10 µm² at 0°, 15° and 30° slant angles. It was 68737.99 µm², 74731.78 µm² and 79541.61 µm² at respective slant angles. In the case of profile roughness as the slant angles increased, the profile roughness increased although the profiling speed decreased. This is due to the increase in cutting/ workpiece thickness. This behavior was observed due to the increased distribution of discharge energy and the variation in gap voltage (Ref 26, 31). The SEM images in Fig. 5(a) show lesser craters, bigger micro-globules, modules, holes, etc., which yields lower profile roughness (0.681 Ra). Figure 5(b) shows more number of smaller craters, larger micro-globules, modules, holes, etc., which gives higher peaks and valleys increasing the profile roughness (0.854 Ra). Similarly, in the case of the highest profiling speed parameters,

Fig. 6(a) shows lesser craters, bigger micro-globules, modules, holes, etc., leading to profile roughness (0.919 Ra) compared to Fig. 6(b). It gives the highest-profile roughness as it has higher peaks and valleys caused by larger micro-globules and modules on the machined surface (1.13 Ra).

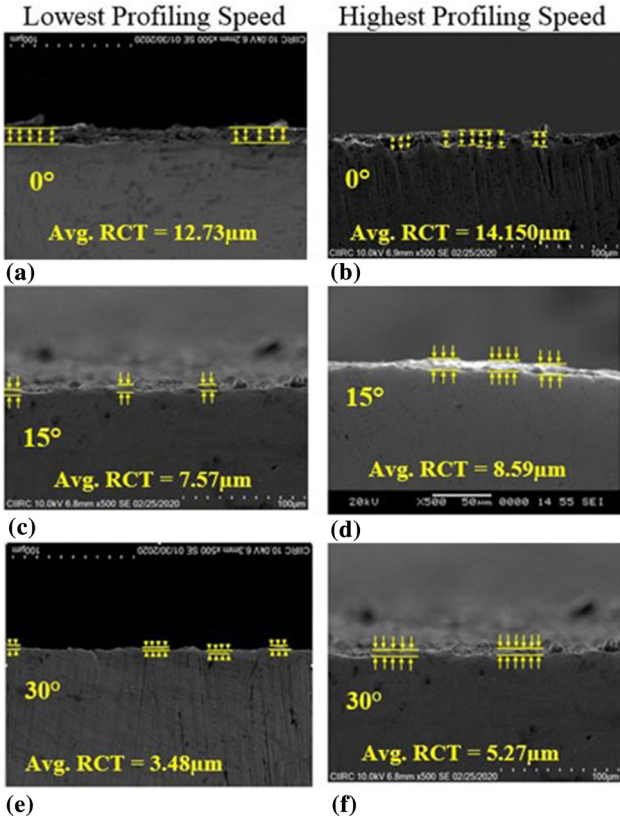


Fig. 7 Variation of recast layer thickness for (a), (c), (e) Lowest and (b), (d), (f) Highest profiling speeds at respective slant angles

3.5 Recast Layer Thickness, Micro-Hardness and Metallurgical Changes in the Profiles

Figure 7(a)-(f) shows the variation of recast layer thickness at different slant angles. This layer was formed due to the resolidification of the melted surface on the parent metal by dielectric fluid after machining. This layer possesses minute voids or porosity in the recast layer, and this was because the gas bubbles get entrapped during solidification which leads to profile roughness as it forms voids on the surface as seen in the SEM microstructure of WED machined surface in Fig. 5 and 6. It was observed that both at the highest and lowest cutting parameters the recast layer thickness decreases as the slant angle increases. This effect was observed because although the discharge energy with which the profiling was performed remains constant the cutting/workpiece thickness increased. Figure 1 shows the increasing cutting thickness as the slant angle increases. As the cutting/workpiece thickness increases, the cooling by dielectric fluid also increases. This leads to the distribution of discharge energy. This distribution of discharge energy decreases the recast layer thickness for higher tapered components. Similar results were observed by Manoj et al. (Ref 26) and Joy et al. (Ref 32) during taper profiling. It was observed that the hardness also decreased as the slant angles increases.

Figure 8 shows the micro-hardness at both the lowest and highest profiling speed parameters. It was noticed that as the slant angle increases the micro-hardness also increased, and at lower slant angles, it recorded the highest. This decreased was noticed due to the metallurgical changes at the machining edge as observed by many researchers (Ref 9, 10, 25, 33, 34). As the slant angles increased, the discharge energy got distributed and the recast layer thickness decreased. Figure 9 shows the EDS results at (a) polished surface before machining, (b) 0°, (c) 15°, and (d) 30° taper components, and Table 3 shows the percentage weight variation of the elements. By EDS in Fig. 9 and Table 3 at different slant angles, we can conclude that as the slant angle increases the Cu, Zn and O also varied which changed the hardness of the component. Similar observations were made by Sharma et al. (Ref 33) during WEDM of Inconel. From the EDS in Fig. 9(a), it can be seen that the polished surface and Fig. 9(b)-(d) surfaces were exposed for machining where the Cu and Zn elements were

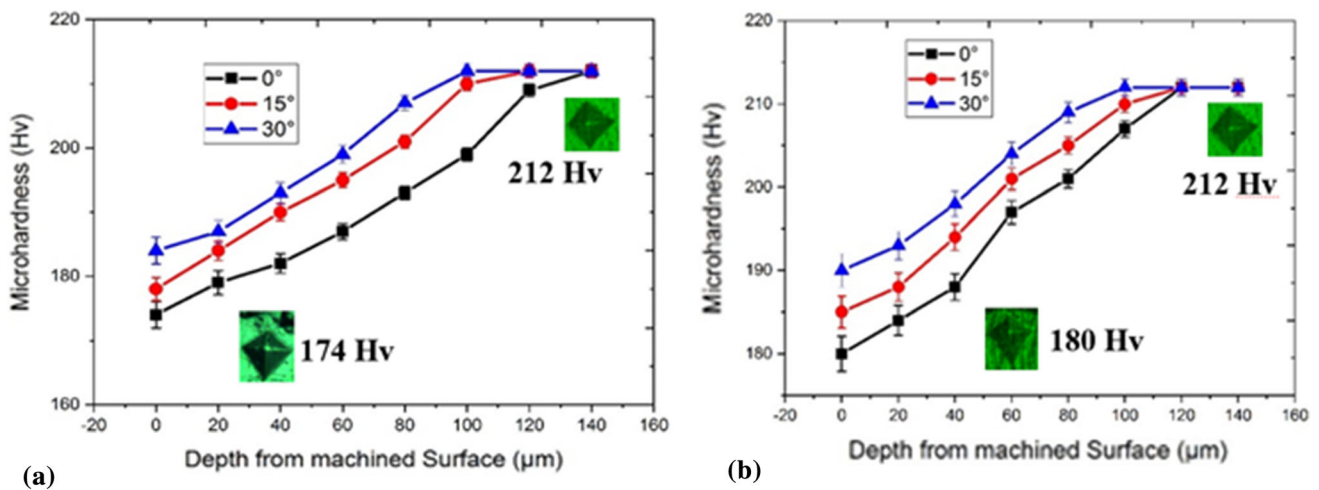


Fig. 8 Micro-hardness at (a) Highest (b) Lowest profiling parameters

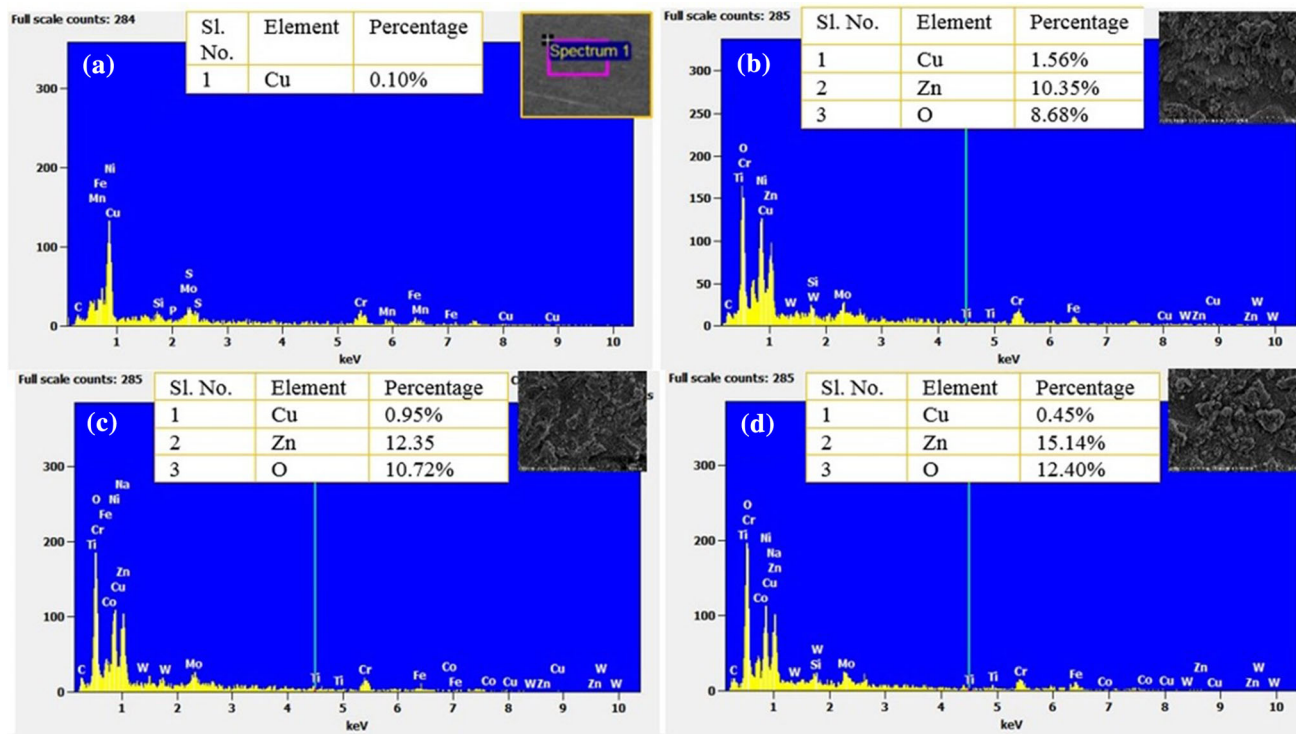


Fig. 9 EDS of (a) Polished material, (b) 0°, (c) 15° and (d) 30° tapered WEDMed surface at highest profiling parameters (WGD = 90 mm, CDT = 99 s, WO = 120 μm, CSO = 100%)

Table 3 Chemical composition of Microfer 4722 superalloy for different slant angles

Sl. No.	Element	Percentage weight, %			
		Polished surface	0°	15°	30°
1	C	0.83	0.72	0.94	1.1
2	Si	1.77	0.97	0.49	0.39
3	Cr	26.71	24.05	24.03	23.02
4	Fe	12.84	12.95	9.98	11.17
5	Ni	35.72	21.89	20.83	19.36
6	Mn	11.54	10.54	10.63	8.73
7	Mo	9.35	7.54	7.67	7.2
8	W	1.23	0.75	1.44	1.4
9	Cu	0.01	1.56	0.95	0.45
10	O	0	8.68	10.72	12.04
11	Zn	0	10.35	12.32	15.14
Total		100	100	100	100

introduced in the parent material by the wire. There is O as the surface was exposed to dielectric fluid soon after the melting. A similar analysis was conducted by Bisaria and Shandilya (Ref 10) during the machining of shape memory alloys. It can be noticed in Fig. 7 that as the slant angle increases the recast layer decreases indicating lesser material degradation (metallurgical changes). This decrease in recast layer and material degradation increases the micro-hardness at higher slant angles compared to 0° slant angles as shown in Fig. 8(a) and (b). Similar results were obtained by Manoj et al. (Ref 26) and Joy et al. (Ref 32) during taper profiling. The 30° taper component recorded the highest WEDMed surface hardness of 182 Hv and 190 Hv at the highest and lowest cutting parameter, whereas 0° taper was

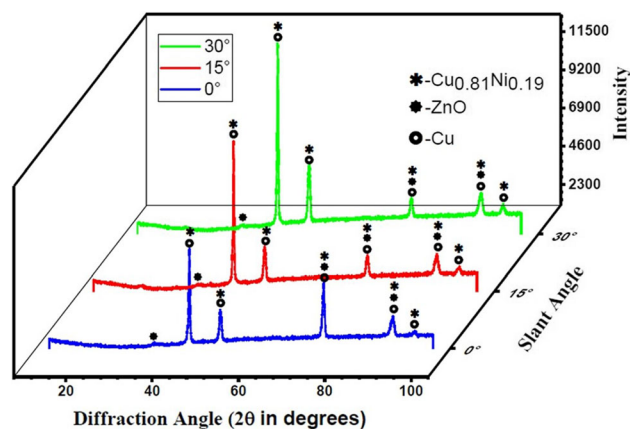


Fig. 10 XRD of machined specimens at different slant angles

recorded with the least hardness of 174 Hv and 180 Hv at the highest and lowest cutting parameter.

3.6 XRD and Residual Stress

The XRD and residual stress analysis were carried out for the profiles machined with the highest profiling parameters (WGD = 90 mm, CDT = 99 s, WO = 120 μm, CSO = 100%). It was observed that Cu, CuNi, and ZnO phases were prominent phases in the peaks by the software as indicated in Fig. 10. It can be observed from the XRD plot that although the machining was performed at the same parameters just by increasing the slant angles the intensity of the peak increases. The intensity of the peak was found to be highest at 30° and lowest at 0° slant angles. Although the discharge energy remains the same (machining parameters remains unchanged),

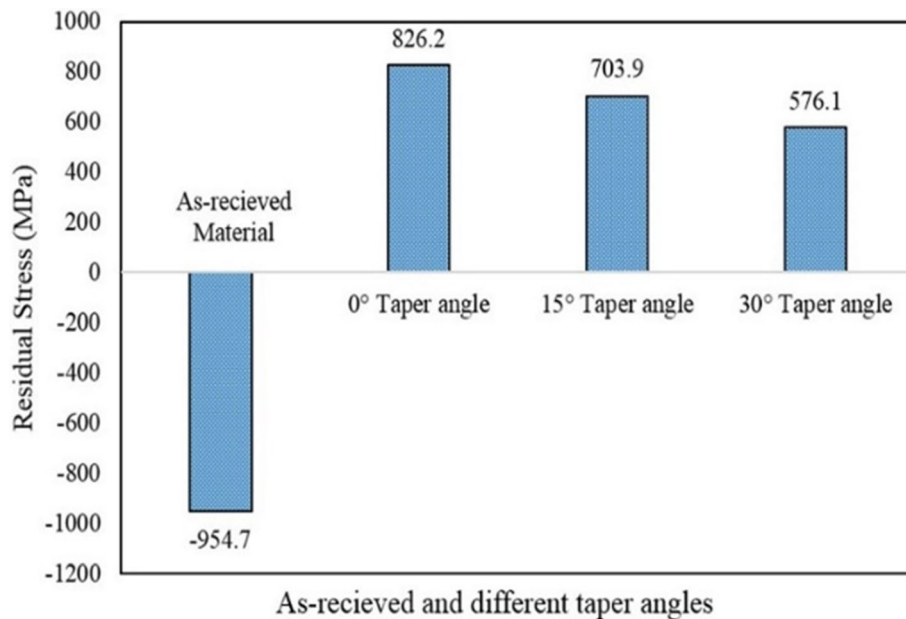


Fig. 11 Residual stress at different slant angles

at higher slant angles due to an increase in workpiece thickness the heat distribution is more. The amount of material melted is lesser which can be observed in both recast layer and micro-hardness. At lower taper, the intensity of the peak is lesser, and this was due to the higher melting of the workpiece. This was due to the lower workpiece thickness and lower cooling from the dielectric fluid. So this infers the reduced crystal size of the WED machined surface at lower slant angles. A similar analogy for different parameters was outlined by Soni et al. and Sharma et al. in their investigations (Ref 11, 34). It can be noticed from XRD Cu, Cu_{0.81}Ni_{0.19} and ZnO phases were prominent which makes the WED machined component softer. The micro-hardness also indicated the softened surface in Fig. 8. The zinc-coated copper wire and dielectric water reacts with the Microfer 4722 forming the phases containing Cu, Zn and O during WEDM. It is observed that there is a slight peak shift toward the right side with increasing the slant angles which indicates the presence of residual stresses as stated by Sharma et al. (Ref 33). The residual stress was measured for as-received metal and WED machined surface at different slant angles. During machining, the sparks are produced due to ionization. These sparks melt the material, and the molten material is carried away as debris. The molten material on the workpiece cools and forms the recast layer. This heating and cooling cycle repeats resulting in residual stress. It was seen initially as-received metal had negative or compressive stresses. At 0° slant angles, the melting is more as the material thickness is lesser compared to the 30° taper. At 30° taper, the melting is lesser due to increased material thickness and cooling will be faster. So, therefore, the heat distribution is more, decreasing the melting of the material and in turn residual stress as shown in Fig. 11. In the case of 0° slant angles, the melting is more as the material thickness is lesser and the heat distribution is reduced. So the residual stress was the highest (826.2 Hv) and the 30° slant angles have the least residual stress (576.1 Hv) as indicated in Fig. 11. The relationship between recast layers is highlighted by Manjaiah M and Rudolph LF where it is stated at higher recast layer thickness the residual stress was the

highest which are tensile compared to other machined zones (Ref 34).

4. Conclusions

From the above study, the output parameters like profiling speed, profile roughness and profiling error were analyzed in taper square profile which were machined on Microfer 4722 superalloy. The input parameters were examined using the one factor at a time approach. The microstructural and corner changes were recorded at the highest and lowest profiling parameters. Further recast layer and hardness were explored at different slant angles. The x-ray diffraction and residual stress analysis were carried out at different slant angles for the highest profiling parameters.

1. Slant angles, wire guide distance, wire offset and cutting speed override were the influential factors in profiling speed, profile roughness and profiling error. The corner dwell time influenced only profiling error. As the cutting speed override parameter controls the discharge energy, it is observed cutting speed override influences the profiling speed significantly. So the highest profiling speed parameters were derived at 100% of cutting speed override parameter and the lowest profiling speed parameters were recorded at 31% of cutting speed override parameter. The profiling roughness also increased with profiling speed because as the profiling speed increases the sparking also increases yielding a surface of higher roughness.
2. As the slant angles increases from 0° to 30°, the profiling speed decreases by 12.53%, and profile roughness and profiling error increases by 22.95% and 15.72% respectively for the highest profiling parameters. A similar trend was found for the lowest profiling parameters where the profiling speed decreased whereas profile roughness and profiling error increased by 26.64%, 25.40% and 10.78%

respectively. These effects in profiling speed, profile roughness and profiling error were observed because of the increase in cutting thickness. As cutting thickness increases, the discharge energy required to melt the material increases, decreasing the profiling speed. The profile roughness increases due to the increased distribution of discharge energy and the variation in gap voltage as cutting thickness increased. In the case of the profiling error, the wire lag increases leading to higher error at corners with the increase in the cutting thickness.

3. As the slant angles increased by 0°–30°, the distribution of discharge energy during machining leads to a decrease in recast layer thickness by 62.76%, 72.66%. The hardness at the machined surface increases by 4.59%, 5.56% at both the highest and lowest parameters, respectively, demonstrating lower material degradation due to machining.
4. The energy-dispersive x-ray analysis and x-ray diffraction analysis confirm the presence of Cu, Zn and O in the machined surface which makes the material softer and this is validated by micro-hardness. During machining the Cu and Zn elements were induced in the parent material by zinc-coated copper wire and O elements were induced due to the dielectric fluid splashed on the melt area for cooling during slant profiling.
5. It was observed in x-ray diffraction analysis that there is a shift in the peaks representing the presence of residual stress. The as-cast material had compressive stresses (– 954.7 Mpa), and the machined samples have tensile stresses. As the slant angles increased from 0° to 30°, the distribution of discharge energy occurs due to an increase in cutting thickness which decreases the residual stresses by 30.27%. This leads to a difference in intensity of the peaks in x-ray diffraction analysis for different slant angles due to the reduced crystal size of the machined surface.

References

1. R. Arunachalam and M.A. Mannan, Machinability of Nickel-Based High Temperature Alloys, *Mach. Sci. Technol.*, 2000, **4**, p 127–168. <https://doi.org/10.1080/10940340008945703>
2. A. Thakur and S. Gangopadhyay, State-of-the-Art in Surface Integrity in Machining of Nickel-Based Super Alloys, *Int. J. Mach. Tools Manuf.*, 2016, **100**, p 25–54
3. V. Baldin, C.R.B. Baldin, A.R. Machado, and F.L. Amorim, Machining of Inconel 718 with a Defined Geometry Tool or by Electrical Discharge Machining, *J. Braz. Soc. Mech. Sci. Eng.*, 2020, **42**(5), p 1–14. <https://doi.org/10.1007/s40430-020-02358-7>
4. H. Bisaria and P. Shandilya, Wire Electric Discharge Machining Induced Surface Integrity for Ni55.95Ti44.05 Shape Memory Alloy, *Proc. Inst. Mech. Eng. Part E J. Process Mech. Eng.*, 2021, **235**, p 178–185
5. H. Bisaria and P. Shandilya, Surface Integrity Aspects for NiTi Shape Memory Alloys During Wire Electric Discharge Machining: A Review, *J. Mat. Res.*, 2020, **35**, p 537–558. <https://doi.org/10.1557/jmr.2020.32>
6. I.V. Manoj, S. Narendranath, and A. Pramanik, Optimization and Prediction of Machining Responses Using Response Surface Methodology and Adaptive Neural Network by Wire Electric Discharge Machining of Alloy-X, *Mater. Sci. Forum Trans. Tech. Publ.*, 2021, **1026**, p 28–38
7. H. Bisaria and P. Shandilya, Processing of Curved Profiles on Ni-Rich Nickel-Titanium Shape Memory Alloy by WEDM, *Mat. Manuf. Process.*, 2019, **34**, p 1333–1341. <https://doi.org/10.1080/10426914.2019.1594264>
8. K. Muralova, J. Kovar, L. Klakurkova, and T. Prokes, Effect of Width of Kerf on Machining Accuracy and Subsurface Layer after WEDM, *J. Mater. Eng. Perform.*, 2018, **27**, p 1908–1916. <https://doi.org/10.1007/s11665-018-3239-4>
9. P. Sharma, D. Chakradhar, and S. Narendranath, Effect of Wire Material on Productivity and Surface Integrity of WEDM-Processed Inconel 706 for Aircraft Application, *J. Mater. Eng. Perform.*, 2016, **25**, p 3672–3681
10. H. Bisaria and P. Shandilya, Experimental Studies on Electrical Discharge Wire Cutting of Ni-rich NiTi Shape Memory Alloy, *Mat. Manuf. Process.*, 2018, **33**, p 977–985. <https://doi.org/10.1080/10426914.2017.1388518>
11. H. Soni, S. Narendranath, and M.R. Ramesh, Effects of Wire Electro-Discharge Machining Process Parameters on the Machined Surface of Ti50Ni49Co1 Shape Memory Alloy, *SILICON*, 2019, **11**, p 733–739
12. K. Muralova, L. Klakurkova, R. Matousek, T. Prokes, R. Hrdy, and V. Kana, Influence of the Cut Direction Through the Semi-Finished Product on the Occurrence of Cracks for X210Cr12 Steel Using WEDM, *Arch. Civ. Mech. Eng.*, 2018, **18**, p 1318–1331
13. Y. Sun, Y. Gong, Y. Liu, M. Cai, X. Ma, and P. Li, Experimental Investigation on Effects of Machining Parameters on the Performance of Ti-6Al-4V Micro Rotary Parts Fabricated by LS-WEDT, *Arch. Civ. Mech. Eng.*, 2018, **18**, p 385–400
14. S. Hatami, M. Shahabi-Navid, and L. Nyborg, Surface Preparation of Powder Metallurgical Tool Steels by Means of Wire Electrical Discharge Machining, *Metall. Mat. Trans. A*, 2012, **43**, p 3215–3226. <https://doi.org/10.1007/s11661-012-1137-1>
15. B. Ahmad and M.E. Fitzpatrick, Minimization and Mitigation of Wire EDM Cutting Errors in the Application of the Contour Method of Residual Stress Measurement, *Metall. Mat. Trans. A*, 2016, **47**, p 301–313. <https://doi.org/10.1007/s11661-015-3231-7>
16. S. Bhattacharya, A. Mishra, N. Keshkar, S. Kumar, V. Kain, and G.K. Dey, Wire Electric Discharge Machining of P91 Steel: Microstructure and Thermal Modeling Studies, *Metall. Mat. Trans. A*, 2019, **50**, p 5336–5355. <https://doi.org/10.1007/s11661-019-05445-0>
17. H. Bisaria and P. Shandilya, Surface Integrity of Ni-Rich NiTi Shape Memory Alloy at Optimized Level of Wire Electric Discharge Machining Parameters, *J. Mater. Eng. Perform.*, 2019, **28**, p 7663–7675. <https://doi.org/10.1007/s11665-019-04477-2>
18. C.A. Huang, G.C. Tu, H.T. Yao, and H.H. Kuo, Characteristics of the Rough-cut Surface of Quenched and Tempered Martensitic Stainless Steel Using Wire Electrical Discharge Machining, *Metall. Mat. Trans. A*, 2004, **35**, p 1351–1357. <https://doi.org/10.1007/s11661-004-0310-6>
19. Narendra Steels Pvt. Ltd, Mumbai. 2010, <http://www.narendrasteels.com/>. (Manufacturer, Exporter and Supplier of nickel superalloys in Mumbai India)
20. H. Chandler, *Heat Treater's Guide Practices and Procedures for Nonferrous Alloys*, 2006 Third Printing
21. T. Chaudhary, A.N. Siddiquee, and A.K. Chanda, Effect of Wire Tension on Different Output Responses During Wire Electric Discharge Machining on AISI 304 Stainless Steel, *Def. Technol.*, 2019, **15**, p 541–544
22. Electronica India Ltd, Operating manual for ELPLUS 15 Ecocut, 2011 Retrieved by email from company, access date: 25-06-2011
23. S. Habib, Optimization of Machining Parameters and Wire Vibration in Wire Electrical Discharge Machining Process, *Mech. Adv. Mater. Mod. Process.*, 2017, **3**, p 1–9. <https://doi.org/10.1186/s40759-017-0017-1>
24. S. Habib and A. Okada, Experimental Investigation on Wire Vibration During Fine Wire Electrical Discharge Machining Process, *Int. J. Adv. Manuf. Technol.*, 2016, **84**, p 2265–2276
25. I.V. Manoj and S. Narendranath, Slant Type Taper Profiling and Prediction of Profiling Speed for a Circular Profile During in Wire Electric Discharge Machining Using Hastelloy-X, *Proc. Inst. Mech. Eng. C J. Mech. Eng. Sci.*, 2021 <https://doi.org/10.1177/0954406221992398>
26. I.V. Manoj, R. Joy, and S. Narendranath, Investigation on the Effect of Variation in Cutting Speeds and Angle of Cut During Slant Type Taper Cutting in WEDM of Hastelloy X, *Arab. J. Sci. Eng.*, 2020, **45**, p 641–651
27. A.B. Puri and B. Bhattacharyya, Modelling and Analysis of the Wire-Tool Vibration in Wire-Cut EDM, *J. Mater. Process. Technol.*, 2003, **141**, p 295–301

28. Z. Chen, Y. Zhang, G. Zhang, and W. Li, Modeling and Reducing Workpiece Corner Error Due to Wire Deflection in WEDM Rough Corner-Cutting, *J. Manuf. Process.*, 2018, **36**, p 557–564
29. S. Sakar, M. Sekh, S. Mitra, and B. Bhattacharyya, A Novel Method of Determination of Wire Lag for Enhanced Profile Accuracy in WEDM, *Precis. Eng.*, 2011, **35**, p 339–347
30. G. Selvakumar, K.G.T. Kuttalingam, and S.R. Prakash, Investigation on Machining and Surface Characteristics of AA5083 for Cryogenic Applications by Adopting Trim Cut in WEDM, *J. Braz. Soc. Mech. Sci. Eng.*, 2018, **40**, p 1–8
31. A. Samanta, M. Sekh, and S. Sarkar, Influence of Different Control Strategies in Wire Electrical Discharge Machining of Varying Height Job, *Int. J. Adv. Manuf. Technol.*, 2019, **100**, p 1299–1309. <https://doi.org/10.1007/s00170-016-9045-y>
32. R. Joy, I.V. Manoj, and S. Narendranath, Investigation of Cutting Speed, Recast Layer and Micro-Hardness in Angular Machining Using Slant Type Taper Fixture by WEDM of Hastelloy X, *Mater. Today*, 2019, **24**, p 1943–1946. <https://doi.org/10.1016/j.matpr.2019.09.021>
33. P. Sharma, D. Chakradhar, and S. Narendranath, Effect of Wire Diameter on Surface Integrity of Wire Electrical Discharge Machined Inconel 706 for Gas Turbine Application, *J. Manuf. Process.*, 2016, **24**, p 170–178
34. M. Manjaiah and L.F. Rudolph, Study on Recast Layer Thickness and Residual Stress During WEDM of SMAs, *Emerg. Mater. Res.*, 2017, **6**, p 82–88

Publisher's Note Springer Nature remains neutral with regard to jurisdictional claims in published maps and institutional affiliations.